Dark Raman resonances due to Ramsey interference in vacuum vapor cells

Z. D. Grujić, M. Mijailović, D. Arsenović, A. Kovačević, M. Nikolić, and B. M. Jelenković*
Institute of Physics, 11080 Belgrade, Serbia
(Received 9 September 2008; published 9 December 2008)

We investigate the evolution of the atomic coherence between Zeeman sublevels with $\Delta m_F=2$ in the region between pump and probe laser beams, in a Rb vapor cell using the Hanle configuration. The transmission of the probe beam, placed inside the hollow pump beam, shows the narrowing of the Hanle resonance (at external magnetic field $B=0$) by Ramsey fringes whose separation from the central peak depends on the distance between the beams. The temporal evolution of the pump induced alignment is evident from the changes of the probe transmission spectra with increasing the angle between linear polarizations of each beam. Experimental results are in agreement with the results of the model which calculates probe fluorescence by solving time-dependent optical Bloch equations, from the time when atom enters the pump beam to the time when it leaves the probe beam. The results for total excited state populations were averaged over atomic velocities distribution.

DOI: 10.1103/PhysRevA.78.063816 PACS number(s): 42.50.Gy, 42.50.Nn, 42.65.−k

I. INTRODUCTION

In coherent population trapping (CPT), laser radiation, applied to a Λ scheme, places atoms in a nonabsorbing or dark state when two light fields are in Raman resonance with the splitting between two lower states [1,2]. This process is very efficient because of simultaneous coherent superposition of the ground states into an absorbing or bright state which is strongly coupled to the excited state of the Λ scheme [3–6]. CPT is observed in fluorescence as a fluorescence dip. Narrow gain in laser transmission or electromagnetically induced transparency (EIT) can be observed due to the existence of the "dark" state.

In this paper, we study EIT resonances in a vacuum vapor Rb cell when we apply Ramsey method [7] of separated excitation regions. We show that such separation of fields plays an important role in line shapes and linewidths of EIT. In the original Ramsey method, long-lived atomic polarization between ground-state hyperfine levels is induced by using microwaves. The first field creates coherent superposition between two levels. In the region between the two fields, coherence acquires a phase shift which depends on both the frequency of hyperfine splitting and the time of flight. The absorption of the microwave field in the second interaction region is modulated if the phase of the coherence is changed, for example, by changing the detuning of the microwaves in respect to the atomic frequency. Temporal instead of spatial separation of microwave Ramsey pulses allows application of Ramsey methods to atomic clocks in buffered alkali-metal gas cells [8]. In our work, we use modified Ramsey method in vacuum Rb cell, by applying pump optical photons to create alignment in the ground-state hyperfine level in a Rb atom, followed by the pair of probe photons to detect induced alignment.

Modified Ramsey methods were performed, in several cases, on thermal atomic beams. Spatially separated pump and probe laser beams, in Raman resonance with two hyperfine levels of the ground state, interact with atoms in Na [9] and Cs [10] atomic beams. Ramsey fringes due to ground-state coherences with $\Delta m_F=2$ were observed in atomic beam of Ca atoms [11]. The observation of Ramsey fringes using nonlinear Faraday rotation spectroscopy (NLFR) in the Rb atomic beam were given in [12]. Experiments [9–12] presented considerably narrower line shapes of EIT and NLFR resonances when compared to nonseparated applied pump and probe beam excitations.

In several works, Ramsey methods were used on beams in Raman resonance to excite alkali-metal atoms, contained in a gas cell and mixed with a buffer gas. Linearly polarized probe beam, counterpropagating vs spatially displaced pump laser beam in sodium vapor, monitors precession of orientation in atoms pumped by the circularly polarized pump laser light [13]. The manifestation of Ramsey interference effect of radio-frequency Zeeman transitions in atomic vapor due to collisional velocity diffusion was shown by Buhr and Mlynek [14,15]. These experiments apply the Ramsey resonance idea in the domain where atoms with CPT alter both their position and velocity. It was shown that multiple collisions between buffer gas atoms and alkali-metal atoms lead to diffusion of alkali-metal atoms back to the laser beam, which leads to diffusion-induced Ramsey narrowing of EIT [16,17]. Temporal Ramsey fringes due to scattering of delayed probe beam by coherently prepared Rb atoms were observed in Ref. [18], while Ramsey fringes due to Zeeman coherence in Rb atoms for temporally and spatially separated laser beams were shown in Ref. [19]. High-contrast, sub-kHz, Ramsey fringes through Raman resonant beams were observed using circularly polarized light and double Λ scheme in Cs vapor with buffer gas [20]. Temporal Ramsey fringes due to multiple atom reflections from coated walls of the Rb cell were measured using both pump and probe beams, spatially overlapped and separated [21].

Excitations from the Ramsey method using beams with Raman resonance in buffered gas cells have found important applications, particularly for CPT based frequency standards and atomic clocks, either active [22,23] or passive [24]. The aim of this paper is to further study Ramsey effects through Raman resonance in vacuum gas cells, i.e., to study the effect

*zoran.grujic@phy.bg.ac.yu

 ©2008 The American Physical Society

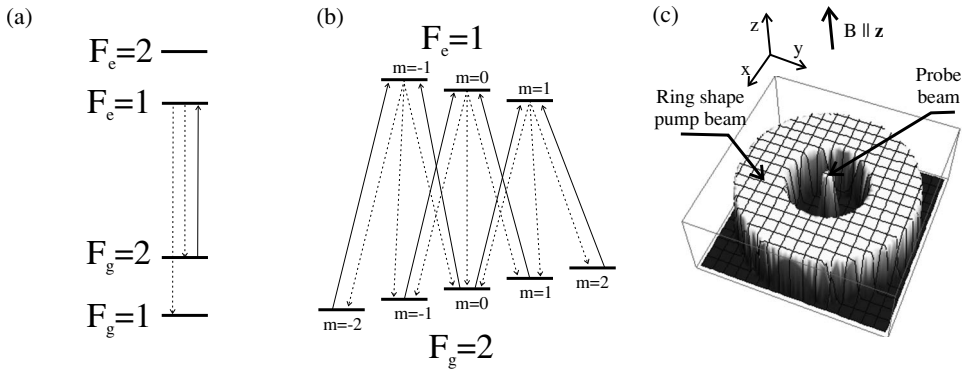

FIG. 1. (a) Schematic of atomic energy level diagram for ^{87}Rb $D1$ line ground and excited levels, (b) the energy level diagram for magnetic sublevels of the $F_g=2\rightarrow F_e=1$ transition, and (c) pump and probe laser beam radial profiles used in the theoretical model. In (a) and (b) solid lines represent laser light coupling energy levels and dotted lines show the deexcitation paths from excited levels.

of the temporal evolution of coherent superposition on the shape of EIT resonance. Similar studies in vacuum cells were briefly done in Ref. [19]. In our work, we use two-photon Raman transitions between Zeeman sublevels of the $F_g=2$ ground-state hyperfine level. Both pump and probe beams are tuned to the $F_g=2\rightarrow F_e=1$ transition in ^{87}Rb and probe beam transmission is monitored while axial magnetic field is scanned around zero. Experimentally, we put the probe beam inside the central region of hollow pump beam. The role of the pump in this setup is similar to that of an antireflection wall coating, and to that of buffer gas collisions in the vapor cell with buffer gas. This setup allows enhanced interaction of the atomic coherence with the probe beam in comparison with separated laser beams [19]. This experimental geometry is similar to the geometry used in Ref. [25], where the sub-Doppler feature was observed in the transmission of the hollow probe, through the very thin (10 μm) cell, while the pump beam is placed in the probe center.

The results of our experiment are compared to the results of time-dependent optical Bloch equations for density matrix elements for atoms in the pump, in the dark, and in the probe region. All the levels interacting with laser light are taken into account, as well as population losses to the other ground-state hyperfine level. Total probe fluorescence was calculated after averaging over atom velocity components parallel and perpendicular to the laser beam. Our work is relevant to some applications of the CPT, particularly for atomic frequency standards based on CPT, either active [22,23] or passive standards [24]. The Ramsey method with Raman resonance type excitation approach has advantages over the standard Ramsey method for atomic frequency standards, since it eliminates need for large microwave resonators.

II. THEORY

We used density matrix formalism to analyze the dynamics of the interaction between Rb atoms and spatially separated pump and probe laser beams. The temporal evolution of the density matrix elements for the excited and the ground state populations and coherences ($\varrho_{e_ie_j}, \varrho_{g_ig_j}$) and for optical coherence ($\varrho_{e_ig_j}$) is obtained from time-dependent optical Bloch equations for the open $F_g=2\rightarrow F_e=1$ transition in ^{87}Rb. Figures 1(a) and 1(b) show Rb atomic level diagrams with levels coupled and optically pumped by laser light.

$$\dot{\varrho}_{e_ie_j} = \varrho_{e_ie_j} i(\omega_{e_j} - \omega_{e_i}) + \frac{i}{\hbar}\sum_{k=-2}^{2}(\tilde{\varrho}_{e_ig_k}E_{+g_ke_j} - E_{-e_ig_k}\tilde{\varrho}_{g_ke_j}) - 2\Gamma_L\varrho_{e_ie_j}\sum_{F_g'}\langle J_g\|e\vec{r}\|J_e\rangle^2(2F_g'+1)(2J_g+1)\begin{Bmatrix} J_g & J_e & 1 \\ F_e & F_g' & I_g \end{Bmatrix}^2,$$

$$\dot{\tilde{\varrho}}_{e_ig_j} = \tilde{\varrho}_{e_ig_j} i[\omega - (\omega_{e_i} - \omega_{g_j})] + \frac{i}{\hbar}\left(\sum_{k=-1}^{1}\varrho_{e_ie_k}E_{-e_kg_j} - \sum_{k=-2}^{2}E_{-e_ig_k}\varrho_{g_kg_j}\right) - \Gamma_L\varrho_{e_ie_j}\sum_{F_g'}\langle J_g\|e\vec{r}\|J_e\rangle^2(2F_g'+1)(2J_g+1)\begin{Bmatrix} J_g & J_e & 1 \\ F_e & F_g' & I_g \end{Bmatrix}^2$$

$$\dot{\varrho}_{g_ig_j} = \varrho_{g_ig_j} i(\omega_{g_j} - \omega_{g_i}) + \frac{i}{\hbar}\sum_{k=-1}^{1}(\tilde{\varrho}_{g_ie_k}E_{-e_kg_j} - E_{+g_ie_k}\tilde{\varrho}_{e_kg_j}) + 2\Gamma_L\langle J_g\|e\vec{r}\|J_e\rangle^2(2F_g+1)(2F_e+1)(2J_g+1)\begin{Bmatrix} J_g & J_e & 1 \\ F_e & F_g & I_g \end{Bmatrix}^2$$
$$\times\sum_{q=-1}^{1}\varrho_{e_{i+q}e_{j+q}}\begin{pmatrix} F_e & 1 & F_g \\ j+q & -q & -j \end{pmatrix}\begin{pmatrix} F_e & 1 & F_g \\ i+q & -q & -i \end{pmatrix}, \quad (1)$$

where

$$E_{+a_i a_j} = -\mu_{a_i a_j -1} E_{-1+} - \mu_{a_i a_j 1} E_{+1+} - \frac{1}{2}\mu_{a_i a_j 0} e^{i\varphi^{zx}} E_{0z},$$

$$E_{-a_i a_j} = -\mu_{a_i a_j -1} E_{-1-} - \mu_{a_i a_j 1} E_{+1-} - \frac{1}{2}\mu_{a_i a_j 0} e^{-i\varphi^{zx}} E_{0z},$$

$$E_{-1+} = \frac{E_{0x} + ie^{i\varphi^{yx}} E_{0y}}{2\sqrt{2}}, \quad E_{-1-} = \frac{E_{0x} + ie^{-i\varphi^{yx}} E_{0y}}{2\sqrt{2}},$$

$$E_{+1+} = \frac{-E_{0x} + ie^{i\varphi^{yx}} E_{0y}}{2\sqrt{2}}, \quad E_{+1-} = \frac{-E_{0x} + ie^{-i\varphi^{yx}} E_{0y}}{2\sqrt{2}}, \quad (2)$$

$\mu_{a_i a_j q}$ is the matrix dipole element, and $\hbar\omega_{e_i}$ and $\hbar\omega_{g_i}$ are the energies of Zeeman sublevels. Fast oscillations at the laser frequency in Eq. (1) were eliminated by common substitution $\varrho_{e_i g_j} = \tilde{\varrho}_{e_i g_j} e^{-i\omega t}$. The summation F'_g is over ground states $F_g = 1, 2$. E_{0x} and E_{0y} are x, y components of the laser's electric vector, orthogonal to the beam propagation direction along the z axis.

$$\vec{E} = \vec{e}_x \cos(\omega t) E_{0x} + \vec{e}_y \cos(\omega t + \varphi^{yx}) E_{0y} + \vec{e}_z \cos(\omega t + \varphi^{zx}) E_{0z}. \quad (3)$$

The identity

$$\sum_{F'_g} (2F'_g + 1) \begin{Bmatrix} J_g & J_e & 1 \\ F_e & F'_g & I_g \end{Bmatrix}^2 = \frac{1}{2J_e + 1} \quad (4)$$

relates Γ_L in Eq. (1) to the emission rate Γ

$$\Gamma = 2\Gamma_L \langle J_g \| e\vec{r} \| J_e \rangle^2 \frac{2J_g + 1}{2J_e + 1}. \quad (5)$$

Here $\langle J_g \| e\vec{r} \| J_e \rangle^2$ is reduced matrix element of the dipole operator between the ground and excited states [26].

As schematically given in Fig. 1(c), the probe laser beam is in the axis of the hollow pump beam. Both the pump and probe beams have the same frequency ω. Their radial intensity profiles are modeled by

$$E(r) = \frac{\mathrm{Erf}\left(\frac{r - r_1}{a(r_2 - r_1)}\right) - \mathrm{Erf}\left(\frac{r - r_2}{a(r_2 - r_1)}\right)}{2}, \quad (6)$$

where r_1, r_2, and a are suitable parameters.

In order to make numerical integration faster, the transition from the region without the laser light to the region with light fields is described by the error function, Eq. (6). External magnetic field B, along the beam propagation, splits the Zeeman sublevels by the amount $2\mu_B g_F B$, where μ_B is the Bohr magneton and g_F is the gyromagnetic factor of the level. We assume that each collision with the wall resets the state of an atom, therefore, atoms entering the pump beam have equal population of Zeeman sublevels in the ground-state hyperfine levels. Numerical integration is carried out until the atom exits the probe region. The density of the rubidium vapor is low enough, so we can ignore relaxation of coherence due to the collision processes.

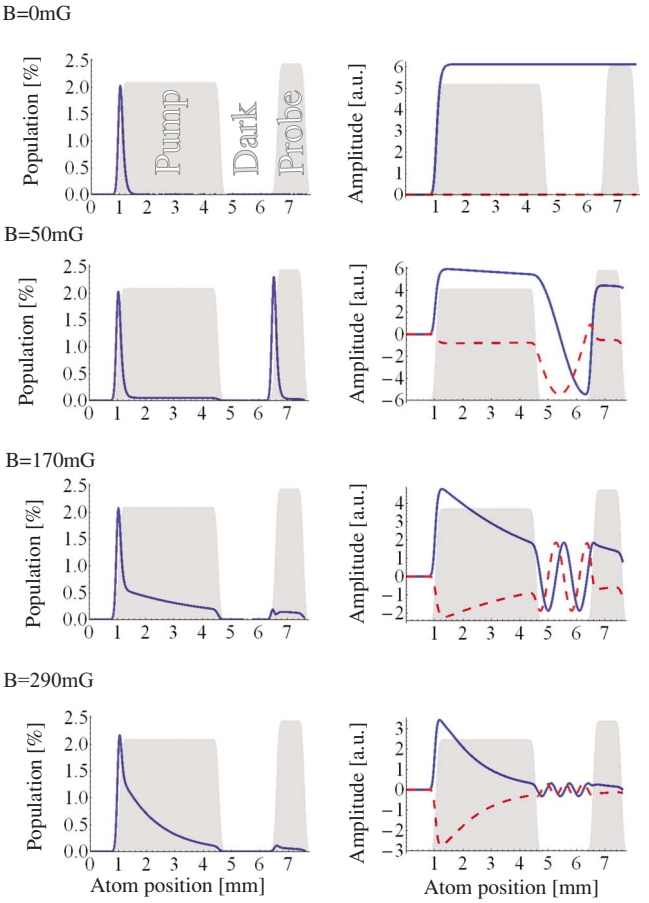

FIG. 2. (Color online) Calculated dependence of spontaneous emission and of ground state coherence between Zeeman sublevels as a function of radial position of an atom (as atom passes through the pump beam, the "dark region," and the probe region) for different values of B. First column: Spontaneous emission from the excited $F_e = 2$ hyperfine level. Second column: the real (solid line) and imaginary (dashed line) parts of Zeeman coherence induced between $m_F = 0$ and $m_F = -2$ Zeeman sublevels of $F_g = 2$. Results are given for the magnetic field values of 0, 50, 170, and 290 mG, for four rows top to bottom and average pump and probe powers of 2 mW and 20 μW, respectively. Polarizations of the pump and probe beam are linear and parallel to each other. The results are for the atom velocity of 260 m/s and its trajectory is along the probe beam diameter. The distances which atoms travel through the pump, "dark" and probe regions are 3.5, 1.7, 1.5 mm, respectively.

The atom fluorescence is proportional to total excited-state population

$$\Pi_e(t, B, \vec{v}) = \sum_i \varrho_{e_i e_i}(t, B, \vec{v}), \quad (7)$$

where $\vec{v}$ is atom velocity vector.

Figure 2 shows the dependence of the atomic fluorescence (left column) and the coherence between Zeeman sublevels $m_F = 0$ and $m_F = -2$ of the $F_g = 2$ (right column) on the atom location for magnetic field B: 0, 50, 170, and 290 mG. Po-

larizations of the pump and probe beam are linear and parallel to each other. As schematically indicated by shaded areas, the atom enters and crosses the pump region, traverses the "dark region" where not illuminated by either of laser fields, and then enters the probe region. Results in Fig. 2 are for the atom velocity of $v=260$ m/s and its trajectory is along the probe beam diameter. Curves presenting $\Delta m = \pm 2$ ground state coherence are real (solid lines) and imaginary (dashed lines) part of the matrix elements $\varrho_{g_i g_j}$. Only for $B=0$, during the flight of atoms through the excitation zone, the excited state population relaxes to zero and the coherence reaches its steady state value. The atom is pumped either into the dark state or to the $F_g=1$ hyperfine level. For $B \neq 0$, the dark state is not ideal. The atom can be excited and then pumped back again either into the dark state or into uncoupled $F_g=1$ hyperfine level. Hence, it is necessary to deal with time-dependent optical Bloch equations not only to take into account the real radial profiles of the pump and probe beams, but also to achieve a proper description of this open atomic system.

Motion of atoms in vacuum Rb cell is faster than the relaxation rates of the ground state coherence and the coherence varies as atoms traverse the pump laser beam. This is in contrast to buffer gas cells where much slower motion of atoms allows the atomic coherence to be instantaneously adjusted at each part of the laser beam [16]. While in the "dark region," the phase of the dark state oscillates, which causes oscillation from dark to bright state. The frequency of the evolution is equal to the separation between Zeeman sublevels, splitted by the $2g_F \mu B$. The frequency of oscillations increases while the amplitudes of modulation decreases with B. In the absence of collisions, the damping rate of the oscillations is zero. For each value of B, the phase shift of the atomic coherence at the entrance of the probe region depends on the atom transit time, which in turn depends on the atom velocity and the direction of the atom propagation. Interference occurs when the electric field of the probe beam, phase coherent to the pump beam, interacts with an atom. If the two oscillators are in phase, the probe beam transmission increases, otherwise decreases. In the cell, the atoms move with different velocities due to the Maxwell-Boltzmann distribution and travel at different angles in respect to the laser beam. Thus, the atoms for the same B acquire different phases at the entrance to the probe beam. This results in the lowering of the amplitude or in the washing out of the Ramsey fringes in the probe transmission.

Total fluorescence from an atom due to excitation by the probe beam is

$$I_e(B,\vec{v}) = \int_0^{t_p} \Pi_e(t,B,\vec{v})dt, \tag{8}$$

where t_p is the atom transit time through the probe beam. This time is determined by the atom trajectory in the probe, i.e., and by velocity component perpendicular to the laser beam v_x. To calculate the total fluorescence $\Upsilon(B)$ we averaged $I_e(B,\vec{v})$ over atom trajectories, i.e., over incident angles of an atom on the probe beam and over different atom velocities ($\vec{v}$ summation). v_z, velocity component parallel with laser beam, determines the Doppler shift in the laser frequency seen by an atom:

$$\Upsilon(B) = \sum_{\vec{v}} |\vec{v}| I_e(B) W_b(T,|\vec{v}|), \tag{9}$$

where $|\vec{v}|$ accounts for atom flux through the laser beam. In Eq. (9)

$$W_b(T,v) = 4\pi \left(\frac{M}{2\pi kT}\right)^{3/2} v^2 e^{-Mv^2/2kT} \tag{10}$$

is the Maxwell-Boltzmann distribution, k Boltzmann constant, T is the temperature of rubidium vapor, and M is the mass of a ^{87}Rb atom. We have found that the contribution to the total fluorescence $\Upsilon(B)$ comes from atoms with small v_z. The range of velocities v_z contributing to the fluorescence increases with the laser beam intensity. Even for the highest intensities, laser detuning as seen by the atom with v_z is much smaller then the separation between the hyperfine levels of the excited $^2P_{1/2}$ state. This justifies why in Eq. (1) we did not include the $F_e=2$ hyperfine level of the excited state.

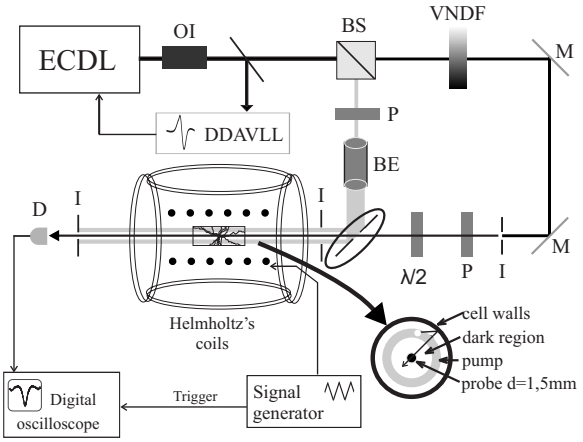

FIG. 3. Experimental setup. ECDL: external cavity diode laser, OI: optical isolator, DDAVLL: Doppler free dichroic atomic laser lock, BS: beam splitter, I: iris, P: polarizer, VNDF: variable neutral-density filter, BE: beam expander, M: mirrors, $\lambda/2$: retardation plate, D: photodiode detector.

III. EXPERIMENTAL SETUP

The laser light is generated by an external cavity diode laser (ECDL) and locked to the $D1$ transition in ^{87}Rb using the doppler free dichroic atomic laser lock (DDAVLL) [27] technique (see Fig. 3). The laser beam is split into two beams using a nonpolarizing beam splitter. The intensities of the two beams are adjusted by variable neutral-density filters. The diameter of one of the beams (the pump beam) is enlarged to ~25 mm and the beam is sent through the iris of 12 mm in diameter. The polarization of the pump beam is determined by the linear polarizer. The linear polarization of the probe beam and its orientation in respect to the linear polarization of the pump beam is determined by both the linear polarizer and a $\lambda/2$ retardation plate. The two beams are combined using a 1-in. mirror with a hole in its center

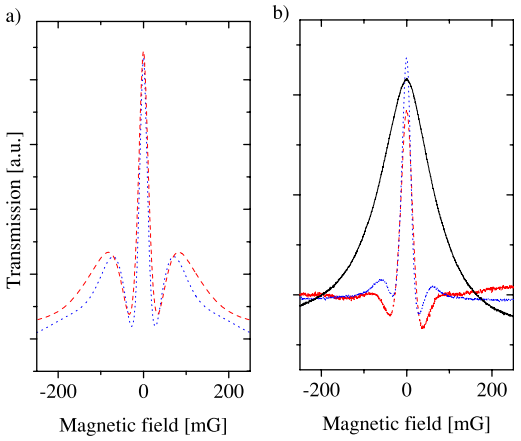

FIG. 4. (Color online) Calculated (a) and measured (b) probe transmission for the $F_g=2\rightarrow F_e=1$ transition in ^{87}Rb as a function of the axial magnetic field. Dashed and dotted lines are for two inner pump beam diameters 5 and 7 mm (corresponding to the "dark region" length of 1.7 and 2.7 mm), respectively. The broad resonance in (b) is for the pump beam turned off (solid line). Both pump and probe beams have the same linear polarization. The probe laser power is 10 μW, while the pump laser power is 0.55 mW.

[28]. The diameter of the hole determines the inner diameter of the pump beam. The probe beam, 1.5 mm in diameter, passes through the center of the hole. Both beams pass through the Rb cell with length of 85 mm and diameter of 25 mm.

The Earth's and laboratory magnetic fields were compensated by three orthogonal pairs of Helmholtz coils. Measured residual inhomogeneity of the total magnetic filed was <5 mG over the cell's length. We generated homogeneous scanning magnetic field B in the direction of the laser beams propagation, by a solenoid around the gas cell.

Behind the cell, the probe beam passes through a circular aperture of the same diameter as the probe beam, in order to eliminate the pump beam contribution to the measured signal at the photodiode. The signal from the photodiode was recorded by the digital oscilloscope while B was scanned around its zero value.

IV. DISCUSSION

In following figures, we compare theoretical and experimental line shapes of the probe Hanle EIT calculated and measured as a function of the external magnetic field B. The direction of the magnetic field is along the laser beam propagation. In the experiment, the magnetic field varies slowly (50 Hz) so that the period of a magnetic sweep is much longer than the atom transit time. The assumption made in the model is that B is constant, while atom passes through three regions (pump, dark, and probe regions). In all figures, spatially displaced pump and probe beams have the same frequency. Figures 4(a) and 4(b) present calculated and measured probe transmission spectra as a function of the axial magnetic field B. The polarizations of the pump and probe beams are linear and parallel. Two circular components of the laser beams interact with two ground-state Zeeman sublevels as schematically shown in Fig. 1(b). Results are given for two lengths of the "dark region," 1.7 and 2.7 mm. As shown in Fig. 4(b), substantial narrowing of the central transmission peak (probe EIT) occurs when the pump beam is on. The probe linewidth is narrower in comparison with the linewidth obtained with the single laser beam whose diameter is similar to the diameter of the pump beam. Longer length of the "dark region" gives narrower EIT peak. Zeeman $\Delta m = \pm 2$ coherence in the $F_g=2$ hyperfine level evolves in the magnetic field (see oscillations in Fig. 2), at the Larmor frequency. The interaction by the probe laser field, in phase with the pump laser field, enters into the interference with the atomic coherence carried by the moving atom. The transmission of the probe beam reflects this interference by the appearance of line shapes with sidebands, i.e., first-order Ramsey fringes. Due to velocity averaging, obtained probe transmission profiles do not show higher-order Ramsey fringes. As seen in Fig. 4(a), the position of fringes slightly changes with the length of the "dark region." When comparing shapes of measured and calculated EIT resonances, one can see very good agreement for the linewidths, while the contrast of measured sidebands is somewhat lost. The inclusion of the influence of the noncoupled ground-state hyperfine level in the optical Bloch equations leads to good agreement for the linewidths. Smaller amplitudes of measured side bands might be due to the measurement procedure: the magnetic field B was swept constantly while the probe transmission was recorded.

EIT resonance line shapes in Fig. 4 are for the probe beam intensity weak enough, so that it does not perturb coherences very much. Since both pump and probe beams couple the same transitions and create Zeeman coherence, increase of the probe power increases its contribution in observed probe EIT. At higher powers, fringes will disappear and the EIT has a central transmission peak on wider pedestal. The pedestal is the probe beam EIT, as shown in Ref. [19].

The evidence of temporal evolution of the coherence was given by measured sensitivity of the probe resonance line shape to the phases of oscillations. In Fig. 5, we present the results for the probe transmission for several angles between the electric vectors of linearly polarized pump and probe beams. The atomic coherence created by linearly polarized pump beam is proportional to $E_p^+E_p^-$, where $E_p^{+(-)}$ are circular $\sigma^{+(-)}$ components of linearly polarized radiation [18,29]. By rotating the polarization of the probe beam by the angle ϕ, we change the phase between the circular components of the pump beam by 2ϕ. This changes the phase of the dark state entering the probe beam for the same amount. For other parameters, such as B and atom velocity, interference will give either narrow transmission gains (for $2\phi=0$) or absorption peak (for $2\phi=\pi$). These two cases are presented by solid and dashed lines, respectively. For other values of ϕ, the transmission has a dispersivelike shape. As the rotation angle increases, the first transmission peak shifts towards higher values of B. This is because by increasing the phase of the pump beam, the dark state interference will occur at higher B. The comparison between results in Figs. 5(a) and 5(b) shows that calculated line shapes are very similar to measured lineshapes.

We use wave forms in Fig. 5 to find the dependence of the first peak position and its amplitude on the pump beam po-

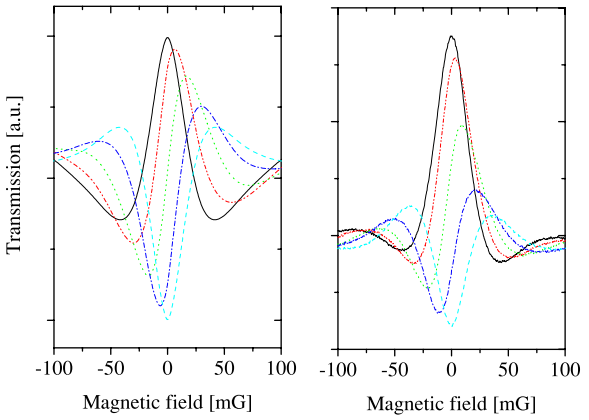

FIG. 5. (Color online) Theoretical (a) and experimental (b) results of probe transmission spectra for the $F_g=2\rightarrow F_e=1$ transition in ^{87}Rb, for linearly polarized pump and probe beams and different probe beam polarization angles in respect to the pump beam polarization (0° solid, 20° dash-dot-dot, 45° dotted, 70° dash-dot, and 90° dashed lines). The probe and pump powers are 20 μW and 1.8 mW, respectively.

larization angle. Figure 6 shows calculated (a) and measured (b) values of B at which this first peak occurs. The results show that the central maximum of the Hanle transmission resonance moves towards higher magnetic fields, as we increase the rotation angle of the probe polarization. Figures 6(c) and 6(d) show the dependence of the amplitude of this peak on the probe beam polarization angle.

V. CONCLUSION

Using the setup of spatially separated, coaxial pump and probe beams we show narrowing of the Hanle EIT resonances in $D1$ transition in ^{87}Rb, due to the Ramsey method with Raman resonance in a vacuum Rb cell. We theoretically explained the shape and the line-widths of experimentally observed EIT resonances by Ramsey interference effects between the phase-oscillating dark state and the probe beam electric filed. These results are of interest for quantum optics of dark states. Placing the probe inside the hole of cylinder-shaped, large-diameter pump beam we also increased the

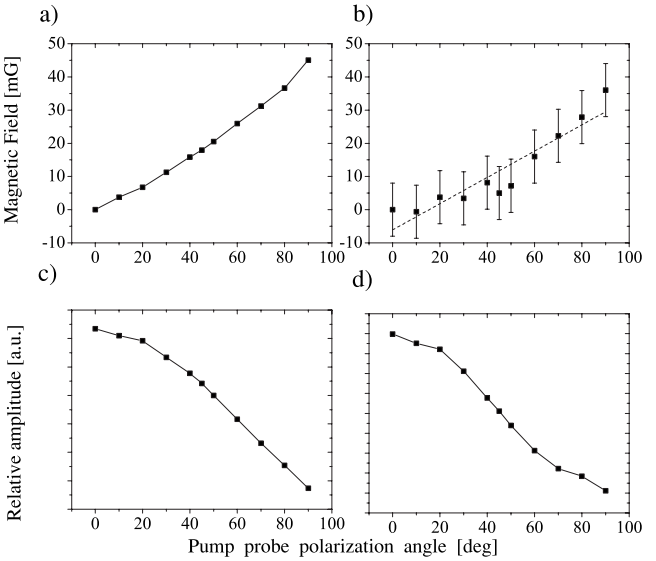

FIG. 6. Theoretical (a) and experimental (b) values of B required to obtain the first transmission peak as a function of the angle of the probe beam polarization. Solid lines are used to guide the eye. Theoretical (c) and experimental (d) variation of EIT amplitude as a function of angle of the probe polarization.

flow of atoms in dark state reaching the probe beam. This setup can be of importance for CPT and EIT applications using vacuum alkali-metal cells in magnetometry. When pump and probe are in Raman resonance with the atom ground states hyperfine splitting, inducing $\Delta m_F=0$ coherence between hyperfine levels, this setup may be of interest for atomic frequency standards. Atomic clocks based on vacuum gas cells are of interest because of temperature sensitive frequency shift in buffer gas cells.

ACKNOWLEDGMENTS

The authors thank S. Cartaleva for useful comments and suggestions. This work was supported by the Ministry of science and environmental protection of the Republic of Serbia, under Grant No. 141003.

[1] G. Alzetta, L. Moi, and G. Orriols, Nuovo Cimento Soc. Ital. Fis., B **52B**, 209 (1979).
[2] E. Arimondo and G. Orriols, Lett. Nuovo Cimento Soc. Ital. Fis. **17**, 333 (1976).
[3] A. Kuhn, S. Steuerwald, and K. Bergmann, Eur. Phys. J. D **1**, 57 (1998).
[4] A. M. Akulshin, S. Barreiro, and A. Lezama, Phys. Rev. A **57**, 2996 (1998).
[5] A. M. Akulshin, S. Barreiro, and A. Lezama, Phys. Rev. Lett. **83**, 4277 (1999).
[6] A. Lezama, S. Barreiro, A. Lipsich, and A. M. Akulshin, Phys. Rev. A **61**, 013801 (1999).
[7] N. Ramsey, *Molecular Beams* (Oxford University Press, London, 1956).
[8] Aldo Godone, Salvatore Micalizio, Filippo Levi, and Claudio Calosso, Phys. Rev. A **74**, 043401 (2006).
[9] J. E. Thomas, P. R. Hemmer, S. Ezekiel, C. C. Leiby, Jr., R. H. Picard, and C. R. Willis, Phys. Rev. Lett. **48**, 867 (1982).
[10] G. Théobald, V. Giordano, N. Dimarcq, and P. Cérez, J. Phys. B **24**, 2957 (1991).
[11] G. Bertuccelli, N. Beverini, M. Galli, M. Inguscio, and F. Strumia, Opt. Lett. **11**, 351 (1986).
[12] B. Schuh, S. I. Konorsky, A. Weis, and T. W. Hänsch, Opt. Commun. **100**, 451 (1993).

[13] S. Nakayama, G. W. Series, and W. Gawlik, Opt. Commun. **34**, 389 (1980).
[14] E. Buhr and J. Mlynek, Phys. Rev. Lett. **57**, 1300 (1986).
[15] E. Buhr and J. Mlynek, Phys. Rev. A **36**, 2684 (1987).
[16] I. Novikova, Y. Xiao, D. F. Phillips, and R. L. Walsworth, J. Mol. Spectrosc. **52**, 2381 (2005).
[17] Y. Xiao, I. Novikova, D. F. Phillips, and R. L. Walsworth, Phys. Rev. Lett. **96**, 043601 (2006).
[18] A. S. Zibrov, I. Novikova, and A. B. Matsko, Opt. Lett. **26**, 1311 (2001).
[19] A. S. Zibrov and A. B. Matsko, Phys. Rev. A **65**, 013814 (2001).
[20] T. Zanon, S. Guerandel, E. de Clercq, D. Holleville, N. Dimarcq, and A. Clairon, Phys. Rev. Lett. **94**, 193002 (2005).
[21] J. Skalla and G. Wäckerle, Appl. Phys. B **64**, 459 (1997).
[22] J. Vanier, Appl. Phys. B **81**, 421 (2005).
[23] L. A. Liew, S. Knappe, J. Moreland, H. Robinson, L. Hollberg, and J. Kitching, Appl. Phys. Lett. **84**, 2694 (2004).
[24] Aldo Godone, Filippo Levi, Salvatore Micalizio, and Claudio Calosso, Phys. Rev. A **70**, 012508 (2004).
[25] S. Briaudeau, S. Saltiel, J. R. R. Leite, M. Oria, A. Bramati, A. Weis, D. Bloch, and M. Ducloy, J. Phys. IV **10**, Pr8-145 (2000).
[26] M. L. Harris, C. S. Adams, S. L. Cornish, I. C. McLeod, E. Tarleton, and I. G. Hughes, Phys. Rev. A **73**, 062509 (2006).
[27] K. L. Corwin, Z. T. Lu, C. F. Hand, R. J. Epstein, and C. E. Wieman, Appl. Opt. **37**, 3295 (1998).
[28] Chang Chun Bo Xin Photoelectric Co., Ltd., Chang Chun, Ji Lin, China, http://www.bxoptic.com/.
[29] M. Fleischhauer, A. B. Matsko, and M. O. Scully, Phys. Rev. A **62**, 013808 (2000).